Journal of Applied Physics

Impedance spectroscopy of Al/AlN/n-Si metal-insulator-semiconductor (MIS) structures

Cite as: J. Appl. Phys. **125**, 084501 (2019); https://doi.org/10.1063/1.5050181
Submitted: 27 July 2018 . Accepted: 06 February 2019 . Published Online: 26 February 2019

Rainer Schmidt, Patrick Mayrhofer, Ulrich Schmid, and Achim Bittner

Journal of Applied Physics ARTICLE scitation.org/journal/jap

Impedance spectroscopy of Al/AlN/n-Si metal-insulator-semiconductor (MIS) structures

Cite as: J. Appl. Phys. **125**, 084501 (2019); doi: 10.1063/1.5050181
Submitted: 27 July 2018 · Accepted: 6 February 2019 ·
Published Online: 26 February 2019

Rainer Schmidt,[1,a)] Patrick Mayrhofer,[2] Ulrich Schmid,[2] and Achim Bittner[3]

AFFILIATIONS

[1]Department of Materials Physics, GFMC, Universidad Complutense de Madrid, Fac. CC. Físicas, 28040 Madrid, Spain
[2]Institute of Sensor and Actuator Systems, TU Wien, Gusshausstrasse 27-29, 1040 Vienna, Austria
[3]Hahn-Schickard, Wilhelm-Schickard-Str. 10, 78052 Villingen-Schwenningen, Germany

[a)]Author to whom correspondence should be addressed: rainerxschmidt@googlemail.com

ABSTRACT

In this work, a comprehensive characterization of metal-insulator-semiconductor structures by impedance spectroscopy is demonstrated for the case of electrically insulating, highly c-axis oriented, 600 nm sputter-deposited AlN films on n-Si substrates with Al top electrodes. Direct visual analysis and equivalent circuit fitting of the dielectric data were performed. For the latter procedure, the circuit model consisted of three series resistor-capacitor connection elements for the three dielectric contributions detected. The three contributions were identified as the AlN film, n-Si substrate, and an interface barrier effect. Several essential device parameters were determined separately, by visual or equivalent circuit fitting analysis, such as the dielectric permittivity of the AlN layer, the temperature dependence of the AlN permittivity, and the resistances of the AlN layer, the n-Si substrate, and the interface contribution. Furthermore, DC bias dependent impedance measurements allowed the identification of a Schottky-type interface barrier.

I. INTRODUCTION

Metal-insulator-semiconductor (MIS) structures are important electronic components that have wide application in the semiconductor industry in coplanar transmission lines,[1,2] diodes,[3,4] and field-effect transistors.[5,6] Most commonly, insulating layers are deposited on semiconducting substrates and metal electrodes are deposited onto the device surface. For the insulating layer, a large variety of different materials can be used ranging from metal oxides like SiO_2,[7] HfO_2,[8] Al_2O_3,[3] and $CaCu_3Ti_4O_{12}$,[9,10] to AlN (bandgap $E_{gap} \approx 6.2$ eV)[11] and BN ($E_{gap} \approx 5.0$ eV).[12] The semiconducting substrate is usually pure or doped Si, whereas the metal component is chosen to be compatible with the insulating layer, i.e., here in this case, Al for AlN. The key component in a MIS structure is the insulating layer, and thus large research efforts have been made to fabricate insulating layers with minimum leakage,[11,13] and optimized thermal[14] and chemical properties that are compatible with the substrate.[15] AlN may be a promising candidate due to its large bandgap, good insulating behavior, a thermal expansion coefficient that is comparable to Si, compatibility with standard CMOS processes, thermal conductivity, and excellent chemical stability.[16–18] Furthermore, AlN thin films show interesting piezoelectric performance, which makes them suitable candidates for application as actuators.[19–21] AlN has also been discussed in the context of micro-machined resonators for viscosity and density sensing of liquids,[22,23] surface acoustic wave applications,[24,25] and blue light emitting diodes.[26]

In this study, the method of impedance spectroscopy has been applied to MIS structures of the composition Al/AlN/n-Si. Impedance spectroscopy is a well-established technique that allows separating different dielectric contributions from different sample areas to the overall dielectric response of functional devices.[27–29] In particular, the resistance and capacitance, or the specific parameters of resistivity and dielectric permittivity, can be extracted separately for different device areas. Therefore, this technique may be ideally suited to analyze MIS structures consisting of electronically different areas. Nevertheless, to the best of the authors' knowledge, impedance spectroscopy has only been applied qualitatively to MIS structures,[9,30,31] but never in a quantitative way with the

aim to extract the separated MIS device parameters. This may in fact be quite surprising since impedance spectroscopy is a well-established technique for the deconvolution and separate analysis of electronically different contributions, and MIS structures are well researched electronic components. However, this lack is probably debited to the fact that the extraction of the resistance and capacitance from the different areas in a MIS structure is a non-trivial task when working only with experimental dielectric data. Here, in this work, it is shown for the first time that a combination of direct visual analysis of the frequency dependent impedance spectroscopy data and equivalent circuit analysis by fitting the data to the adequate model is indeed a viable way to extract all relevant MIS device parameters separately.

For the case of an Al/AlN/n-Si MIS structure, it is found that the impedance spectra contain contributions from the highly c-axis oriented 600 nm AlN layer, the n-Si substrate, and an interface barrier effect, where the resistivity and the dielectric permittivity could be determined separately for each contribution. Generally, a high resistivity or low leakage is desired in the insulating layer of a MIS structure, which can be achieved by optimum thin film deposition conditions, avoiding the formation of structural defects, pin-holes, impurities, or other irregularities. It is shown here that the reliable detection of the separated AlN layer resistivity is possible by alternating current (AC) impedance spectroscopy, whereas direct current (DC) measurements would be dominated by the highly insulating interface barrier resistance that can be resolved only at high temperature (T). Furthermore, for piezoelectric and transistor applications, a low T-dependence of the AlN dielectric permittivity is desired, which can be detected unambiguously and independently from other dielectric contributions by impedance spectroscopy.

II. IMPEDANCE SPECTROSCOPY

Alternating current (AC) impedance spectroscopy experiments consist of an electric stimulus in terms of a time (t)-dependent alternating voltage signal U of variable angular frequency $\boldsymbol{\omega}$ and fixed amplitude $\mathbf{U_0}$ applied to the sample: $U(\omega, t) = \mathbf{U_0}\cos(\boldsymbol{\omega}\, t)$. Effectively, the amplitude I_0 and phase shift δ of the alternating current response I are measured over a wide frequency range: $I(\omega, t) = I_0\cos(\boldsymbol{\omega}\, t - \delta)$. The impedance response from one specific area in a solid sample can be represented by an equivalent circuit element consisting of a parallel resistor-capacitor connection (RC element).[32,33] This RC element model can be understood intuitively: The application of a voltage stimulus to a solid sample leads to two instant and concurrent responses of the sample, i.e., dielectric polarization of localized charges and charge transport of mobile charge carriers. Considering the example of an RC element representing an insulating material, the capacitor describes the polarizability of the material and its ability to store charge, and the parallel resistor describes the sample's resistance that arises from the charge transport of mobile charge carriers that bypass or "escape" the ideal charge storage element.

A MIS structure is expected to contain several electronically very distinct contributions, where each may be represented by one RC element. The simplest overall equivalent circuit describing the macroscopic impedance response would be made up of a series connection of the corresponding RC elements, if the impedance is measured in a parallel-plate electrode configuration with all MIS contributions connected in series.

It is demonstrated here that a combination of two different ways of analyzing the frequency dependent dielectric data from Al/AlN/n-Si MIS structures allows extraction of the most important dielectric MIS device parameters: (i) the AlN permittivity, (ii) the T-dependence of the AlN permittivity, (iii) the insulating resistivity of the AlN layer, (iv) the resistance of the insulating interface, and (v) the resistance of the semiconducting n-Si substrate: (A) Direct visual analysis of the data leads to the highest precision for determining the AlN permittivity and its T-dependence, whereas (B) fitting the data to an equivalent circuit model consisting of three series RC elements leads to precise AlN, n-Si, and interface resistance values over certain T-ranges where a valid fit can be obtained. In the case presented here, it turned out that equivalent circuit fitting is preferential for obtaining resistance values due to lower fitting errors and the wider T-ranges covered as compared to direct visual analysis of the data, e.g., by estimating the size of impedance arcs. Furthermore, direct current (DC) bias dependent impedance spectroscopy measurements allowed identifying a Schottky type interface barrier.

This impedance analysis employed here may generally be viable to comprehensively characterize MIS structures in terms of the relevant device dielectric parameters, which in turn allows a detailed assessment of the functionality and potential application performance of the respective MIS structure devices.

In order to account for the non-ideality of dielectric contributions using equivalent circuit fitting, the ideal capacitors in each RC element may be replaced or complemented by constant-phase elements (CPEs), sometimes also denoted as Q-elements, leading to R-CPE and R-CPE-C,[34,35] or RQ and RQC elements. It is interesting to note that R-CPE elements are in fact compatible with Jonscher's universal response law.[36,37] The complex impedances Z* of ideal RC, non-ideal R-CPE, and R-CPE-C elements are, respectively, given by

$$Z^*(RC) = \frac{R}{1 + i\omega RC}; \quad Z^*(R-CPE) = \frac{R}{1 + (i\omega)^n RC'}; \quad Z^*(R-CPE-C) = \frac{R}{1 + (i\omega)^n RC' + i\omega RC}, \tag{1}$$

$i = \sqrt{-1}$, R and C correspond to the resistance and capacitance of ideal resistors and capacitors, n (<1) is a critical exponent indicating the non-ideality of the respective dielectric contribution (in the ideal case, $n = 1$), and C' is a specific capacitance for a CPE. The definitions and the physical meaning of CPE-containing circuit components are explained in more detail in Sec. I of the supplementary material.

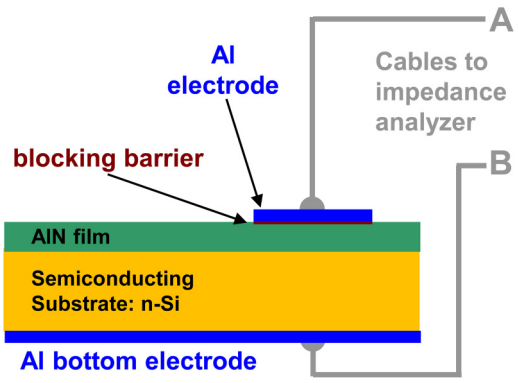

FIG. 1. Schematic sketch of the parallel plate electrode configuration for AC impedance spectroscopy measurements on an Al/AlN/n-Si MIS structure.

In equivalent circuit fitting procedures on real dielectric data, it is often required to change the RC element for one specific dielectric contribution from RC to R-CPE and to R-CPE-C elements at different T, depending on the distribution of relaxation times τ that may change with T or, more importantly, depending on how much of a dielectric contribution is in fact visible in the data over the f-range available at the respective temperature. In semiconducting or insulating materials, a dielectric contribution can often be fitted with an ideal RC or almost ideal R-CPE element (n = close to 1) at low T (high resistances), where the resistance may have to be set to infinity. By increasing T, the resistance may become accessible at some point, the CPE exponent may decrease considerably below 1, and at even higher T a switch to an R-CPE-C element can sometimes be necessary. By further increasing T, the respective dielectric contributions may again move out of the available f-range, and the same consecutive changes to the equivalent circuit may be necessary but in the reverse order (R-CPE-C, R-CPE, RC). In Sec. II of the supplementary material, the different equivalent circuit models applied here at different T-ranges are presented and discussed, and in Sec. IV all fitted parameters extracted from the equivalent circuit fits are summarized.

It should be noted at this point that the well-known Debye model may not be adequate to extract the relevant dielectric parameters for MIS structures as is argued in Sec. III of the supplementary material.

In order to obtain the specific parameters of resistivity and dielectric permittivity, the resistance and capacitance values extracted from the fits were normalized by the geometrical factor g. The AlN film thickness was used as the electrode distance d and the area A of the Al top-electrodes as the current cross section and g is then given by $g = A/d$. The measurement setup is depicted in Fig. 1.

III. EXPERIMENTAL

The deposition of highly c-axis oriented 600 nm thick granular AlN layers onto (100) n-type Si wafers by DC sputtering has been described in previous publications.[16,17,38] For AC impedance spectroscopy measurements, Al top electrodes (1 mm diameter) were deposited onto the AlN surfaces. Furthermore, the backsides of the 525 μm thick n-Si substrates were fully covered with Al, as depicted in Fig. 1, to perform out-of-plane impedance measurements along the film normal axis in a parallel-plate capacitor configuration.[39–41] Impedance spectroscopy measurements were carried out at variable temperature (T) between 180 K and 570 K (−93 °C–297 °C) using a Novocontrol Alpha-A High Performance Frequency Analyzer equipped with a liquid nitrogen cooled sample chamber. A 100 mV amplitude alternating voltage signal of various frequencies (f) between 10 mHz and 10 MHz was employed. At T = 560 K, several f-dependent impedance spectra were measured with different DC bias voltages (0, 1, 2, 3, 5, 7.5, 10, 15, 20 V), which were superimposed over the 100 mV AC amplitude using the standard routine available from the Novocontrol equipment.

Impedance data were obtained at each T in terms of the real and imaginary parts (Z', Z'') of the complex impedance $Z^* = Z' + iZ''$. The data were converted into the notations of complex dielectric permittivity $\varepsilon^* = \varepsilon' - i\varepsilon''$ and conductivity $\sigma^* = \sigma' - i\sigma''$ using the standard conversion: $Z^* = (i\omega C_0 \varepsilon^*)^{-1} = (\sigma^*)^{-1}$, where C_0 is the capacitance of the empty measurement cell. Equivalent circuit fitting of the impedance data was performed by employing the commercial Z-View® fitting software, where the equivalent circuit model was fitted to both the real and imaginary parts of the f-dependent impedance data by minimizing the statistically weighted linear least-squares. f-dependent data were collected at steady-state conditions at various fixed T, where T was allowed to settle for several minutes before measuring an impedance spectrum. The values extracted from the equivalent circuit fits were plotted versus T in various notations, but only the values were considered that were extracted from fits with sufficiently low fitting errors (<5%). Data structuring, analysis, and visualization including the experimental and fitted curves was carried out using the custom built software (Visual Basic) that was developed within the Impedance Spectroscopy Consulting (ISC) consortium.

IV. RESULTS AND DISCUSSION

A. Dielectric permittivity versus f

The f-dependent impedance spectroscopy data collected at various T from the Al/AlN/n-Si MIS structure are shown comprehensively in the format of the real part of the dielectric permittivity ε' vs f in Fig. 2. Most data points fall onto one plateau of a value of $\varepsilon' \approx 10.5$, which is in reasonable agreement with the dielectric permittivity of AlN reported previously.[42,43]

Therefore, the dielectric contribution associated with this plateau in ε' vs f can be associated with the AlN layer. In the adapted equivalent circuit model, the AlN was represented by an R1-CPE1 at low T, and at higher T by an R1-CPE1-C1 element to obtain optimum fits (see Sec. II of the supplementary material). Note that the experimental data were normalized to the AlN layer thickness and top-electrode

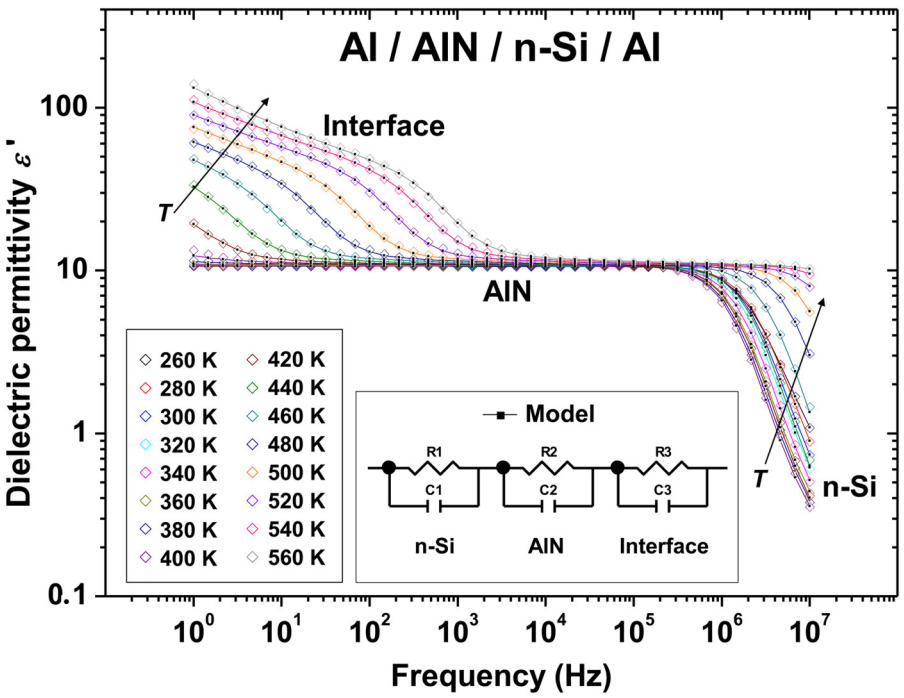

FIG. 2. Dielectric permittivity ε' *vs* f at various T. Three dielectric contributions (AlN, n-Si, Interface) are detected and can be fitted with a model based on three series RC elements (the idealized RC elements are shown in the figure inset). For valid fits, the idealized RC elements were adapted and replaced by R-CPE or R-CPE-C elements, as discussed in Sec. II of the supplementary material. ◇ correspond to the data, and -■- correspond to the adapted equivalent circuit model. Black arrows indicate increasing T.

area, whereas the ε' values below 1 for the n-Si contribution at high f are unphysical and result from the unknown geometry of the n-Si contribution.

At higher T and low f, an interface related contribution appears, whereas at lower T and high f, an additional dielectric contribution originating from the semiconducting n-Si substrates can be observed. The assignments of the total of three dielectric contributions to the AlN film, the n-Si substrate, and to an interface barrier will all be justified in more detail throughout this manuscript by considering the extracted resistivity and permittivity values and their trends with T and the applied DC bias. The n-Si contribution was represented in the adapted equivalent circuit model by an R2-C2 or R2-CPE2 element and the interface contribution by an R3-CPE3 or R3-CPE3-C3 element (see Sec. II of the supplementary material).

The connection of the three RC elements in series (see Fig. 2, inset) is a result of the series arrangement of the three different components of the MIS structure using the top-bottom parallel plate electrode configuration displayed in Fig. 1. In Fig. 2, good agreement between data and model is displayed at all T investigated. The good agreement was confirmed in all other notations of the impedance data, i.e., for the complex impedance Z''-Z', permittivity ε'-ε'', and conductivity σ'-σ''.

No signs of any inductive contribution were encountered, i.e., the imaginary part of the impedance Z'' always displayed negative and the real part of the permittivity ε' always positive values. This implies that the impedance spectra are always dominated by capacitive contributions in the sample and inductive contributions from the measurement cables and other extrinsic sources are not accessible. In particular, the contribution from the semiconducting n-Si substrate appears at high f and masks any potential inductive contributions, which would also be expected to appear at high f.[39] The contribution from the semiconducting n-Si substrate is expected to appear at high f due to the relatively low resistance and small time constants and the resulting faster conduction process. Inductive contributions generally have an

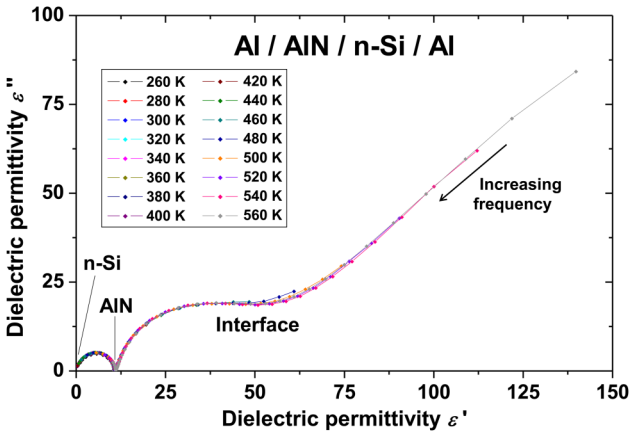

FIG. 3. Cole–Cole plots of imaginary part of the dielectric permittivity ε'' *vs* ε' at various T.

impedance Z* that increases with f ($Z^* = i\omega L$), which is not what was observed in the data.

B. Cole-Cole plots

An alternative representation of impedance spectroscopy data is the Cole-Cole plot of the imaginary part of the permittivity ε'', sometimes denoted as dielectric losses, *versus* the real part ε'. Figure 3 shows two semicircles and one slightly inclined low frequency pike, which is precisely the behavior expected for a series connection of three non-ideal RC elements.

The data all fall approximately on one curve. The fitted curves are not shown for clarity. The permittivity values of AlN and n-Si contributions are indicated by solid lines. The black arrow indicates increasing frequency.

The diameters of the two semicircles correspond to the differences between the different permittivity values of the AlN layer, n-Si substrate, and interface contribution, which can also be deduced from Fig. 2. The AlN and n-Si permittivity values are indicated by solid lines, where such permittivity values may be better assessed in Fig. 4 showing a magnification of the AlN/n-Si semicircle. It is interesting to note that the data for all T fall approximately on one curve, which has some important implications. The dimensions of the two semicircles displayed are approximately independent of T, which in turn implies that the capacitance of the AlN layer, n-Si substrate, and the interface all show no or only weak T-dependence as expected. Furthermore, Fig. 3 indicates that the dielectric loss ε'' is an f-dependent parameter, which is dominated by different dielectric contributions at different f and T. This would also apply to the loss tangent $\tan\delta$ ($= \varepsilon''/\varepsilon'$).

It can be further concluded that the dimensions of the two semicircles displayed are approximately independent of the resistors R1, R2, and R3, which all display considerable T-dependence as is demonstrated in Sec. IV D. This is particularly significant for the ε'' values at specific f and T, since ε'' values are referred to as the dielectric losses and are supposed to indicate the leakage behavior, which in turn is directly related to the resistance. However, the ε'' values at the peak frequency ε'' (f_{max}) only depend on the size of the semicircle, which in turn depends on the difference between the ε' permittivity values, i.e., in the case of the AlN/n-Si semicircle ε'' (f_{max}) $\approx (\varepsilon'_{AlN} - \varepsilon'_{n\text{-}Si})/2$. Only the peak frequencies f_{max} where the Cole-Cole semicircles have their maxima depend in a complicated way on the resistances of both contributions that make up the respective semicircle, e.g., R1 and R2 for the AlN/n-Si semicircle. All these arguments support the approach of fitting the dielectric data presented here to an equivalent circuit consisting of series RC elements, which may generally be favorable for extracting the resistance or leakage behavior of dielectric contributions, as compared to a detailed analysis of ε'' and/or $\tan\delta$.

Figure 4 indicates that the AlN/n-Si semicircle is slightly suppressed below the ε' real axis, which is the typical behavior of non-ideal dielectric contributions that can be accounted for by the use of CPEs. The real ε' x-axis intercepts are highlighted by solid perpendicular lines in Fig. 4 and correspond to the AlN film and n-Si substrate permittivity values as indicated. The exact values for the n-Si substrate permittivity needed to be extrapolated down to the ε'-axis intercept, which was achieved by using the fitting software. However, the n-Si permittivity values obtained would be associated with relatively large fitting errors (5%–40%, depending on T and the exact model used) and would be physically meaningless due to the unknown substrate geometry. The AlN

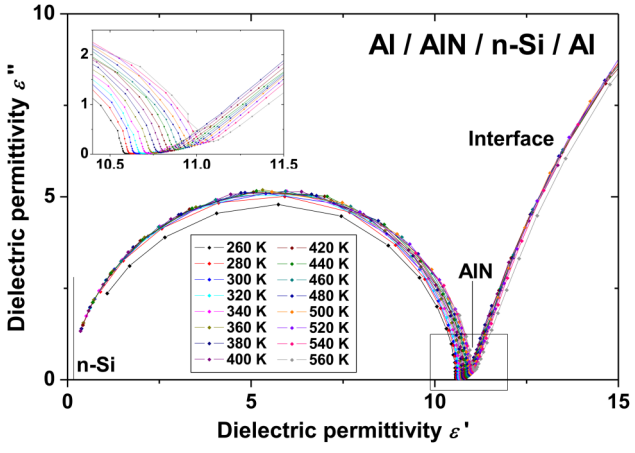

FIG. 4. Magnification of Fig. 3 (ε'' *vs* ε') at high f at various T. The figure inset shows a further magnification as indicated by the solid square near the local minima that correspond to the AlN permittivity ε', displayed on the real ε' x-axis.

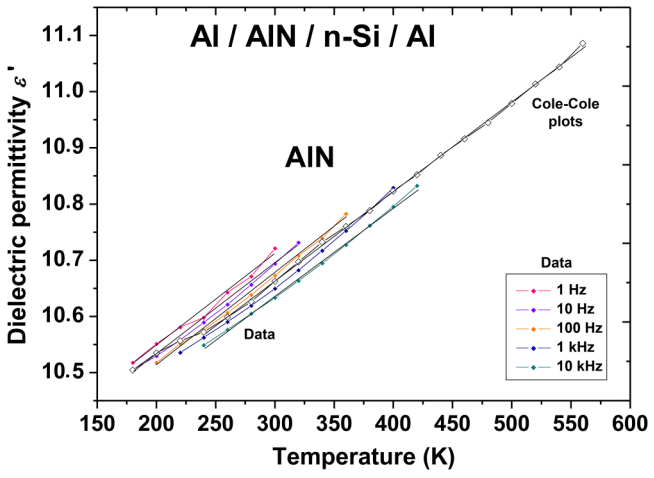

FIG. 5. Real part of permittivity ε' *vs* T for the AlN contribution. The data were determined from (i) the minima in the Cole-Cole plots (see the inset of Fig. 4) and (ii) the raw data in the linear intermediate f regime, where the AlN contribution is dominant (see Fig. 2). A small T-dependence of the AlN permittivity is indicated. Black solid lines are guide to the eyes to indicate good linearity and similar slopes.

permittivity is again indicated to be ≈10.5, in agreement with Figs. 2 and 3 and reports from the literature.[42,43] Figure 4 (inset) shows a further magnification of the real ε'-axis intercept that corresponds to the AlN permittivity. The minimum or point of inclination can be interpreted as the AlN permittivity on the real ε'-axis, and a small T-dependence of the AlN layer permittivity is indicated. This T-dependence of the AlN permittivity is depicted in more detail in Fig. 5. The ε' vs T values for the AlN layer were directly extracted from the minima or points of inclination in the Cole-Cole plots (Fig. 4, inset) in form of a direct visual analysis of the data, where such values are shown together with the raw measured data at various f as indicated.

All ε' vs T curves show good linearity with approximately identical slopes, which constitutes a good confirmation that the assignation of the minima or points of inclination in the Cole-Cole plots to the AlN permittivity may be reasonable. Figure 5 also shows that the method of determining the AlN permittivity from the Cole-Cole plots leads to a more comprehensive picture over a wider T-range. It is therefore proposed that the Cole-Cole plots and their minima may be an ideal tool to assess the T-dependence of the permittivity in AlN layers within a MIS structure directly by visual analysis. The slope of the ε' vs T curve from the Cole-Cole plots is 0.0015383 K^{-1}, which corresponds to a permittivity or capacitance (C) shift with T of $\Delta\varepsilon'/\varepsilon'$ or $\Delta C/C \approx 0.0154\%$ per Kelvin, which is in a similar range as the values reported previously for polycrystalline AlN sintered substrates (≈0.0105% per Kelvin).[44]

It should be noted at this point that the changes in capacitance $\Delta C/C$ between two temperature intervals of 20 K for impedance measurements are considerably lower as compared to the fitting errors of the RC element capacitors or CPEs in the equivalent circuit model of 0.5%–3%. Therefore, the trends of C vs T or ε' vs T are displayed with significantly better linearity and less noise by extracting the ε' permittivity values directly and visually from the data, rather than using the values extracted from equivalent circuit fits.

C. Al/AlN Schottky barrier and interface resistance

The possible formation of a Schottky interface barrier was investigated by applying a DC voltage signal that was superimposed onto the 100 mV amplitude AC signal used for impedance spectroscopy. At a fixed temperature of 560 K and by increasing the DC bias, a significant drop in dielectric permittivity ε' was observed at low f, where the interface contribution is dominant (see Fig. 6). The low-f data cut-off in Fig. 6 increases to higher f with increasing DC bias, whereas at lower-f, the data would be dominated by measurement noise.

This is due to the resolution limit of the impedance measurement apparatus in the respective configuration used. The decrease of permittivity at low-f with DC bias is well known to be a typical feature of Schottky barriers that commonly occur at electrode–sample interfaces or at grain boundaries (GBs).[45–48] Figure 6 (inset) shows the ε' vs f curves again over a wider f-range and without applied DC bias at selected T for comparison.

Furthermore, the applied DC bias has a distinct effect on the conductivity σ', which is displayed in the representation of σ' vs f, with different applied DC biases at 560 K in Fig. 7 (inset), and without DC bias in Fig. 7. Figure 7 (inset) shows that the increasing DC bias leads to a distinct increase in conductivity at low f where the interface contribution is dominant, which is again a typical feature of Schottky barriers. The

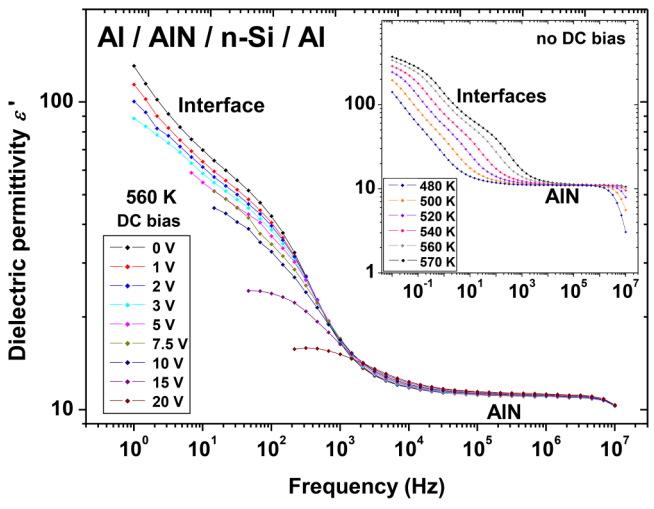

FIG. 6. Dielectric permittivity ε' *vs* f data (◆) at 560 K under applied DC bias. The interface permittivity decreases with increasing DC bias, which is the typical behavior of a Schottky barrier. The inset shows ε' *vs* f at various T near 560 K without DC bias for comparison.

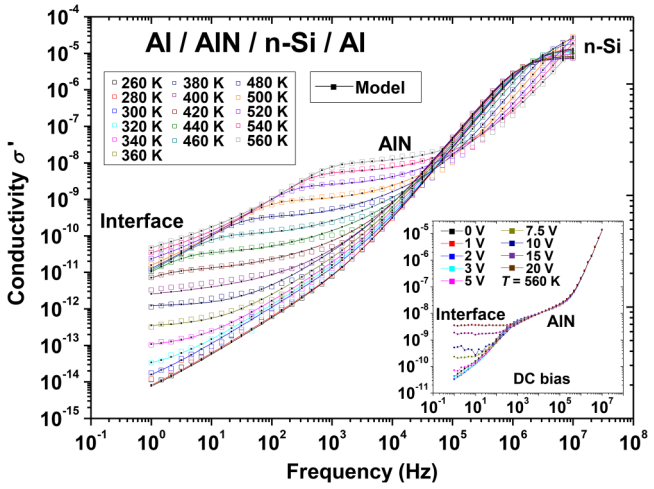

FIG. 7. Real part of the conductivity σ' *vs* f at various T. The contributions from interface, AlN, and n-Si contributions are indicated. □ correspond to the data, and -■- correspond to the adapted equivalent circuit model. The figure inset shows σ' *vs* f data (■) at 560 K under applied DC bias. The strongly increasing interface conductivity with DC bias is the typical behavior of a Schottky barrier.

increasing DC bias has the effect here of increased current injection from the metallic electrodes across the potential barriers at the interfaces. The explanation of Schottky barriers occurring at GBs is not plausible, because in pure AlN no n- or p-doping is evident. Therefore, the formation of Schottky barriers at the GBs is not likely nor is it commonly reported for AlN and related materials. Furthermore, it should be considered that the AlN films investigated here in this work are highly c-axis oriented and may therefore be electronically homogeneous.

The dielectric contribution at low-f displayed in Figs. 2 and 7 may more likely be associated with an electrode interface barrier, which is represented by the R3-C3 element in the idealized equivalent circuit model shown in Fig. 2. It may be argued that the interface may most likely arise at the Al/AlN junction rather than at the AlN/n-Si interface, because Schottky type interfaces may most likely occur at metal–insulator interfaces, where the mismatch of work functions may be most significant. The ideal R3-C3 element that represents this interface had to be adapted to a R3-CPE3 or R3-CPE3-C3 element for valid fits, as mentioned above and demonstrated in Sec. II of the supplementary material.

In Fig. 7 again, all three dielectric contributions of the MIS structure can be identified in the σ' vs f curves, in particular in form of conductivity plateaus for the n-Si and AlN contributions. The fact that the σ' vs f curves show a clearly defined plateau at the high-f end implies that the conductivity of the n-Si contribution can be extracted reliably from the equivalent circuit model (see Fig. 2) with sufficiently low fitting errors (0.1%–6.1% depending on T).

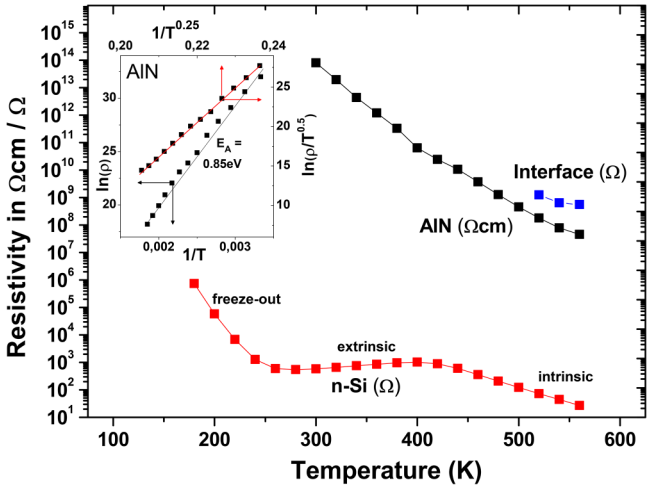

FIG. 8. Resistivity (Ω cm) and resistance (Ω) vs T as extracted from the resistors R1, R2, and R3 in the equivalent circuit model. The interface resistance is high and only accessible at high T, which indicates a blocking interface barrier. In the inset, the data for the AlN layer are plotted on Arrhenius ln(ρ) vs 1/T and on VRH ln($\rho/T^{0.5}$) vs $1/T^{0.25}$ axes, where the linearity is superior on the latter.

On the other hand, the interface contribution shows the signs of a σ' plateau only at low f at the highest measured temperatures of 520 K–560 K, where the fitting errors for the corresponding resistor (R3) strongly increase at lower T. This implies that the equivalent circuit model gives reliable measures of the interface resistance R3 only at 520 K–560 K. For fits at $T < 480$ K, the interface resistance R3 in the equivalent circuit model was set to infinity to obtain valid fits. The data in Fig. 7 are shown together with the fitted curves, which all show excellent agreement.

D. T-dependence of the resistors R1, R2, and R3

The resistance values of the three dielectric contributions of the MIS structure encountered here were extracted with the best precision (lowest fitting errors) from the respective resistors in the equivalent circuit model and are presented in Fig. 8. The resistance R2 from the n-Si substrate (red curve) shows the typical T-dependence of n-Si, which justifies the association of this dielectric contribution and the respective R2-C2 (see Fig. 2) or R2-CPE2 element to the n-Si substrate. The respective R-T curve shows the freeze-out, extrinsic, and intrinsic charge transport regions as expected. Contrarily, the AlN resistivity (R1) and interface resistance (R3) show insulating behavior.

It should be noted that the AlN resistance was normalized by the geometrical factor g containing film thickness and electrode sizes. This leads to specific units of resistivity ρ (Ω cm), whereas the specific units are not accessible for the n-Si and interface contributions. In this case, the nominal values in units of resistance (Ω) are displayed in Fig. 8, for n-Si and interface contributions. Due to this normalization, the R-T curves for AlN and the interface contribution seem to be similar in terms of the nominal resistance. However, this is a false picture because the interface areas may be expected to be thin as compared to the film thickness of 600 nm, and the interface resistivity ρ would then be several orders of magnitude higher as compared to the nominal interface resistance R3 displayed in the R vs T curve. On the other hand, using the specific ρ units (Ω cm), the AlN ρ vs T curve may be a viable tool to assess the true leakage behavior of the AlN layer at various T, separated from all other contributions. By plotting the AlN film resistivity ρ vs T on Arrhenius axes (lnρ vs 1/T), an activation energy (E_A) of ≈0.85 eV can be found (see Fig. 8, inset, left, and bottom axes). This E_A value is considerably lower as compared to the direct bandgap of monocrystalline AlN (6.2 eV), which points toward a leakage conduction mechanism that may be dominated by defects and/or impurities. This finding of impurity dominated conduction is supported by the fact that the linearity of the Arrhenius plot can be improved considerably by representing the data on variable-range hopping (VRH) axes of $\ln(\rho/T^{0.5})$ vs $1/T^{0.25}$, where VRH is a typical charge transport model for impurity dominated conduction. The exponent of 0.25 is commonly associated with Mott-VRH.[49] The alternative Efros-Shklovskii VRH model[50] of $\ln(\rho/T)$ vs $1/T^{0.5}$ gives inferior linearity. It should be considered though that Mott-VRH is a special case of the Efros-Shklovskii

model for a constant density of electron states around Fermi-level without a Coulomb gap.[51]

It is noted at this point that the VRH-type conduction in the AlN layer can be detected only by the application of impedance spectroscopy, which allows separating the AlN layer resistivity from all other contributions to the dielectric data such as the highly resistive interface. This is clearly evident by considering the Al/AlN interface resistance. This resistance (in Ω) is displayed only between 520 K and 560 K in Fig. 8, because at lower T the resistance is too high and hence cannot be extracted from the equivalent circuit model as mentioned above. This implies that the Al/AlN interface resistance is dominating over the AlN layer resistance and DC measurements for Al/AlN/n-Si MIS structures would therefore be inadequate to characterize the leakage of the AlN film. Furthermore, the high DC resistance may not even be resolved at all or only at 520 K–560 K using conventional DC measurements.

V. CONCLUSIONS AND DISCUSSION

Deconvolution and separate analysis of three dielectric contributions in Al/AlN/n-Si MIS structures was achieved by the use of AC impedance spectroscopy, where the contributions were identified as (i) the intrinsic AlN film contribution, (ii) n-Si substrate, and (iii) an interface contribution. By using an appropriate equivalent circuit model and by direct visual analysis of the dielectric data, it is possible to determine the relevant device parameters from MIS structures separately: here, in this case, the AlN film, n-Si and interface resistance, the AlN dielectric permittivity, and all their specific T-dependencies. Charge transport in the AlN film is consistent with VRH, which is a model that is frequently applied to describe impurity conduction in conventional semiconductors. Furthermore, it is possible to identify a Schottky-type interface barrier most likely at the Al/AlN interface, which shows the typical variations in conductivity σ' vs f and permittivity ε' vs f with applied DC bias.

The approach presented here in this work allows a separate analysis of the dielectric permittivity and the resistivity of the AlN layer, which allows detailed judgement on the suitability of the AlN as an insulating layer within Al/AlN/n-Si MIS structures. By considering the conventional f-dependent dielectric leakage parameters ε'' or tan δ ($= \varepsilon''/\varepsilon'$), it may be possible to characterize the AC leakage of a simple device driven solely in AC mode at a given f. However, this approach may be unsuitable in the MIS structures presented here, where three dielectric contributions are dominant at different f. In particular, the curves ε'' vs f or tan δ vs f would be dominated by the interface resistance at certain f, which is inconvenient to judge on the leakage of the insulating AlN layer. To conduct research and development work toward improved MIS structures for potential applications, for example, by studying systematically the factors that reduce the leakage of the AlN layer or increase its resistivity, a separate analysis of the different MIS structure components is required, which can be achieved by AC impedance spectroscopy. DC resistance measurements may be unsuitable for Al/AlN/n-Si MIS structures, because the DC resistance would be dominated by the extrinsic interface contribution. Therefore, AC impedance spectroscopy may be regarded as the method of choice to analyze the dielectric properties of MIS structures for each dielectric contribution separately.

SUPPLEMENTARY MATERIAL

See the supplementary material for (I) constant phase elements (CPEs), (II) equivalent circuit models used in this study, (III) Debye equivalent circuit model, and (IV) parameter extracted from the equivalent circuit models.

ACKNOWLEDGMENTS

R.S. wishes to thank Jacobo Santamaría, Carlos León, and Alberto Rivera-Calzada for allowing us to use and help with the Novocontrol impedance analyzer.

REFERENCES

[1]T. Shibata and E. Sano, IEEE Trans. Microw. Theory Tech. **38**(7), 881–890 (1990).
[2]A. Sakr, W. Dyab, and K. Wu, in *2016 16th Mediterranean Microwave Symposium* (MMS) (IEEE, Abu Dhabi, 2016), pp. 1–4.
[3]T. Manago and H. Akinaga, Appl. Phys. Lett. **81**(4), 694–696 (2002).
[4]T. Yamamoto and M. Morimoto, Appl. Phys. Lett. **20**(8), 269–270 (1972).
[5]S. Sasa, M. Ozaki, K. Koike, M. Yano, and M. Inoue, Appl. Phys. Lett. **89**(5), 053502 (2006).
[6]M. A. Khan, X. Hu, A. Tarakji, G. Simin, J. Yang, R. Gaska, and M. S. Shur, Appl. Phys. Lett. **77**(9), 1339–1341 (2000).
[7]L. Messick, J. Appl. Phys. **47**(11), 4949–4951 (1976).
[8]W. J. Zhu, M. Tso-Ping, T. Tamagawa, J. Kim, and Y. Di, IEEE Electron Device Lett. **23**(2), 97–99 (2002).
[9]G. Deng, T. Yamada, and P. Muralt, Appl. Phys. Lett. **91**(20), 202903 (2007).
[10]G. Deng, Z. He, and P. Muralt, J. Appl. Phys. **105**(8), 084106 (2009).
[11]F. Engelmark, J. Westlinder, G. F. Iriarte, I. V. Katardjiev, and J. Olsson, IEEE Tran. Electron Devices **50**(5), 1214–1219 (2003).
[12]H. Miyamoto, M. Hirose, and Y. Osaka, Jpn. J. Appl. Phys. **22**(4), L216 (1983).
[13]N. B. Hassine, D. Mercier, P. Renaux, G. Parat, S. Basrour, P. Waltz, C. Chappaz, P. Ancey, and S. Blonkowski, J. Appl. Phys. **105**(4), 044111 (2009).
[14]O. Ambacher, J. Phys. D Appl. Phys. **31**(20), 2653 (1998).
[15]S. Strite and H. Morkoç, J. Vac. Sci. Technol. B **10**(4), 1237–1266 (1992).
[16]M. Schneider, A. Bittner, and U. Schmid, Sens. Actuators A Phys. **224**, 177–184 (2015).
[17]M. Schneider, A. Bittner, A. Klein, and U. Schmid, Microelectron. Eng. **140**, 47–51 (2015).
[18]A. Ababneh, H. Kreher, and U. Schmid, Microsyst. Technol. **4–5**, 567–573 (2008).
[19]R. Mahameed, N. Sinha, M. B. Pisani, and G. Piazza, J. Micromech. Microeng. **18**(10), 105011 (2008).
[20]M.-A. Dubois and P. Muralt, Sens. Actuators A Phys. **77**(2), 106–112 (1999).
[21]M. Fischeneder, M. Oposich, M. Schneider, and U. Schmid, Sensors **18**(11), 3842 (2018).
[22]G. Pfusterschmied, M. Kucera, E. Wistrela, T. Manzaneque, V. Ruiz-Díez, J. L. Sánchez-Rojas, A. Bittner, and U. Schmid, J. Micromech. Microeng. **25**(10), 105014 (2015).
[23]G. Pfusterschmied, M. Kucera, W. Steindl, T. Manzaneque, V. Ruiz Díez, A. Bittner, M. Schneider, J. L. Sánchez-Rojas, and U. Schmid, Sens. Actuators B Chem. **237**, 999–1006 (2016).

[24]M. B. Assouar, M. El Hakiki, O. Elmazria, P. Alnot, and C. Tiusan, Diam. Relat. Mater. **13**(4), 1111–1115 (2004).
[25]H. P. Loebl, C. Metzmacher, R. F. Milsom, P. Lok, F. van Straten, and A. Tuinhout, J. Electroceram. **12**(1), 109–118 (2004).
[26]A. Dadgar, M. Poschenrieder, J. Bläsing, K. Fehse, A. Diez, and A. Krost, Appl. Phys. Lett. **80**(20), 3670–3672 (2002).
[27]E. Barsukov and J. R. Macdonald, *Impedance Spectroscopy: Theory, Experiment and Applications* (John Wiley & Sons Inc., Hoboken, 2005).
[28]R. Schmidt, in *CRC Concise Encyclopedia of Nanotechnology*, edited by B. Kharisov, O. Kharissova, and U. Ortiz-Mendez (CRC Press, Taylor & Francis Group, Boca Raton, 2015).
[29]J. Ryu, D. Park, and R. Schmidt, J. Appl. Phys. **109**(11), 113722 (2011).
[30]M. Okutan and F. Yakuphanoglu, Microelectron. Eng. **85**(3), 646–653 (2008).
[31]Y. Şafak Asar, T. Asar, Ş Altındal, and S. Özçelik, Philos. Mag. **95**(26), 2885–2898 (2015).
[32]J. T. S. Irvine, D. C. Sinclair, and A. R. West, Adv. Mater. **2**(3), 132 (1990).
[33]J.-G. Ramírez, R. Schmidt, A. Sharoni, M. E. Gómez, I. K. Schuller, and E. J. Patiño, Appl. Phys. Lett. **102**(6), 063110 (2013).
[34]E. J. Abram, D. C. Sinclair, and A. R. West, J. Electroceram. **10**, 165 (2003).
[35]C. H. Hsu and F. Mansfeld, Corrosion **57**(9), 747 (2001).
[36]A. K. Jonscher, *Dielectric Relaxation in Solids* (Chelsea Dielectrics, London, 1983).
[37]R. Schmidt and A. W. Brinkman, J. Appl. Phys. **103**(11), 113710 (2008).
[38]M. M. Schneider, A. Bittner, and U. Schmid, J. Phys. D Appl. Phys. **48**(40), 405301 (2015).
[39]R. Schmidt, W. Eerenstein, T. Winiecki, F. D. Morrison, and P. A. Midgley, Phys. Rev. B **75**, 245111 (2007).
[40]E. Langenberg, L. Maurel, N. Marcano, R. Guzmán, P. Štrichovanec, T. Prokscha, C. Magén, P. A. Algarabel, and J. A. Pardo, Adv. Mater. Interfaces **4**(9), 1601040 (2017).
[41]R. Schmidt, J. Ventura, E. Langenberg, N. M. Nemes, C. Munuera, M. Varela, M. Garcia-Hernandez, C. Leon, and J. Santamaria, Phys. Rev. B **86**(3), 035113 (2012).
[42]A. T. Collins, E. C. Lightowlers, and P. J. Dean, Phy. Rev. **158**(3), 833–838 (1967).
[43]N. Kuramoto, H. Taniguchi, and I. Aso, IEEE Trans. Compon. Hybrids Manuf. Technol. **9**(4), 386–390 (1986).
[44]J. S. Thorp, D. Evans, M. Al-Naief, and M. Akhtaruzzaman, J. Mater. Sci. **25**, 4965 (1990).
[45]X. Guo and R. Waser, Prog. Mater. Sci. **51**(2), 151–210 (2006).
[46]B. L. Sharma, *Metal-Semiconductor Schottky Barrier Junctions and Their Applications* (Plenum Press, New York and London, 2013).
[47]C. S. Hwang, B. T. Lee, C. S. Kang, K. H. Lee, H.-J. Cho, H. Hideki, W. D. Kim, S. I. Lee, and M. Y. Lee, J. Appl. Phys. **85**(1), 287–295 (1999).
[48]J. P. McKelvey, *Solid State and Semiconductor Physics* (Harper & Row, New York, 1966).
[49]N. F. Mott, *Conduction in Non-Crystalline Materials* (Clarendon Press, Oxford Science Publications, Oxford, 1993).
[50]B. I. Shklovskii and A. L. Efros, *Electronic Properties of Doped Semiconductors* (Springer-Verlag, Berlin, 1984).
[51]R. Schmidt, A. Basu, and A. W. Brinkman, Phys. Rev. B **72**(11), 115101 (2005).